RESEARCH ARTICLE v130

Hybrid amyloid-based redox hydrogel for bioelectrocatalytic H_2 oxidation

Nicolas Duraffourg,[a] Maxime Leprince,[a] Serge Crouzy,[a] Olivier Hamelin,[a] Yves Usson,[b] Luca Signor,[c] Christine Cavazza,[a] Vincent Forge[a] and Luca Albertin*[a]

Dedicated to the memory of Dr. Serge Crouzy

[a] Dr N. Duraffourg, M. Leprince, Dr. S. Crouzy, Dr O. Hamelin, Dr C. Cavazza, Dr V. Forge, and Dr L. Albertin
Univ. Grenoble Alpes, CEA, CNRS, IRIG, LCBM, 38000 Grenoble, France
E-mail: luca.albertin@cea.fr
[b] Dr. Y. Usson
Univ. Grenoble Alpes, CNRS, CHU Grenoble Alpes, Grenoble INP*, TIMC-IMAG, 38000 Grenoble, France
[c] Dr. L. Signor
Univ. Grenoble Alpes, CEA, CNRS, IRIG, IBS, 38000 Grenoble, France

Supporting information for this article is given via a link at the end of the document.

Abstract: An artificial amyloid-based redox hydrogel was designed for mediating electron transfer from a [NiFeSe] hydrogenase to an electrode. Starting from a mutated prion-forming domain of fungal protein HET-s, a hybrid redox protein featuring a single benzyl methyl viologen moiety was synthesized that is capable to self-assemble into structurally homogenous nanofibrils. Molecular modelling confirmed that redox groups are aligned along the fibril's axis, and tethered to its core via a long flexible polypeptide chain that allows close encounters among the fibril-bound oxidized/reduced redox groups. Redox hydrogel films capable of immobilizing the hydrogenase at the surface of carbon electrodes under mild conditions were obtained by simple pH jump. Based on these properties, new bioelectrodes for the electrocatalytic oxidation of H_2 were fabricated that afforded catalytic current densities of up to 270 µA cm^{-2} under quiescent conditions at 45°C.

Introduction

Efficient electrocatalysts are needed in technological applications ranging from energy conversion and storage, to biofuel cells; to the production of electrofuels, commodity chemicals and materials. [1] In nature all biological systems extract energy and nutrients from their environment, and carry out metabolic processes associated with life, with high atom and energy efficiency. Redox enzymes - a particular class of biocatalysts – catalyse many of the reactions involved in these processes, and the design, fabrication, and use of enzyme-modified electrodes is an active field of research. [2]

Enzymatic bioelectrocatalysis holds the promise of i) higher energy efficiency (i.e. lower applied overpotentials); ii) elimination of organic solvents from the electrolyte; iii) extreme product selectivity - which removes the need for downstream purification processes; and iv) limited or no use of precious metals.

The major challenge in bioelectrocatalysis is to establish electrical communication between enzymes and electrode surfaces: [1a] most enzymes have an active centre buried deep beneath their surface and surrounded by an insulating protein shell, which prevents direct electron transfer (DET) with the electrode. [3]

Though DET is easier for enzymes with built-in electron transfer pathways, such as hydrogenases, [4] the enzyme still needs to be adsorbed on the surface of the electrode with appropriate orientation, so that the most accessible relay centre is close enough to the electrode to allow electron tunnelling. [5]

Redox hydrogels – i.e. cross-linked polymer networks featuring reversible redox moieties tethered to their backbone chains - are the only electron-conducting phase in which water-soluble chemicals and biochemicals dissolve and diffuse. [6] Accordingly, they are of much interest in bioelectrocatalysis since they can wire to the electrode a high number of embedded enzyme molecules, irrespective of their spatial orientation and distance, while allowing the diffusion of reactants, products and ions to and from the bulk of the solution. Moreover, self-standing redox hydrogel films immobilize the biocatalyst within a hydrophilic and solvated matrix that protects it from denaturation. [7]

Amyloid-based hydrogels (AbHs) [8] are water-swollen, three-dimensional networks formed by cross-linking of protein fibrils with a structure rich in cross-β-sheets. [9] The exact mechanism of gelation is complex and varies from one system to another, but it involves a combination of non-covalent interactions (i.e. hydrogen bonding, hydrophobic and electrostatic interactions) and fibrils' entanglement. [8, 9c, 10] The ability of AbHs to hold large amounts of water is due to the great number of hydrophilic and charged functional groups present on the surface of protein fibrils. Together with viscoelasticity, these physical properties make AbHs good mimics of the cytosol, extracellular matrix, and biofilms in which many enzymes and bacteria have evolved and/or normally function. Hence, development of electron-conducting AbHs would enable their use as biomimetic immobilizing matrices in bioelectrocatalysis.

* Institute of Engineering Univ. Grenoble Alpes

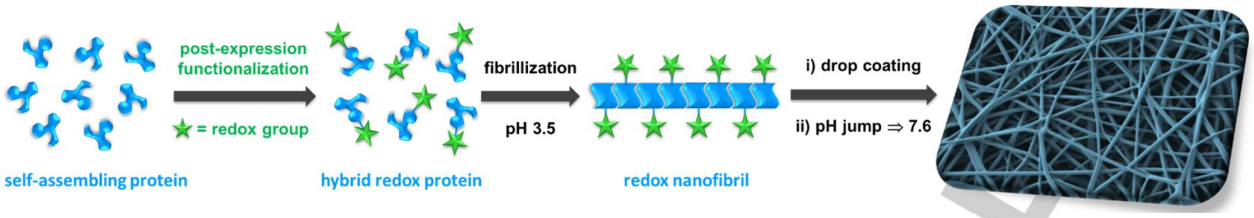

Scheme 1. Synthesis of redox nanofibrils from a self-assembling hybrid protein and preparation of amyloid-based redox hydrogel films.

In 2006, Dobson, Barker and *coll.* [11] first proposed the use of amyloid fibril scaffolds to display redox proteins in a linear array in order to favour inter-protein electron transfer via conformational sampling at the protein–protein interface and, ultimately, electron transfer over long distances. [12]

Holzinger, Forge and *coll.* [13] applied this concept to the preparation of protein nanowires featuring a contiguous alignment of metalloproteins on their surface. To this end, they exploited the ability of the prion-forming domain (PFD, residues 218 to 289) of the protein HET-s from fungus *P. anserina* (HET_{PFD}) [14] to self-organize into amyloid fibrils with high structural homogeneity, and to do so in a reproducible way even when fused to another domain of comparable size.[15] Hence they constructed a fusion protein comprising a small rubredoxin from *Methanococcus voltae* connected to the *C*-terminus of HET_{PFD}. Following a pH jump, these nanowires self-assembled into redox hydrogel films capable to mediate electron-transfer between an electrode and an imbedded laccase or [NiFe] hydrogenase.

This work elegantly demonstrated the possibility to develop amyloid-based redox hydrogels (AbRxHs) and to use them in bioelectrocatalysis. In theory, by changing the nature of the metalloprotein displayed on the fibrils' surface, one could design AbRxH spanning the whole potential window of redox proteins, *i.e.* -700 to +700 mV vs SHE, [16] thus allowing their adoption in a wide range of electrochemical devices. [7] In practice, the need to purify the PFD-containing fusion protein under denaturing conditions limits its scope to redox domains that are either extremely stable or that can be easily refolded in their holo form once the chaotropic agent removed. Also, (i) the active centre of the redox domain has to be close enough to the surface as to allow effective interprotein electron transfer; (ii) its longitudinal size along the fibril axis shall not lead to steric hindrance and prevent self-association of the fusion protein; and (iii) a new fusion protein has to be designed, expressed, and refolded whenever the potential of the redox matrix has to be changed.

A more versatile approach to AbRxHs (Scheme 1) involves:

(i) production of a self-associating protein carrying one or more functional group(s) amenable to orthogonal chemical functionalization;

(ii) site-selective conjugation of artificial prosthetic group(s) (e.g. metal complex or organic molecule) possessing redox or catalytic properties matching the target application;

(iii) self-association of the resulting hybrid construct into redox nanofibrils and gels.

Thus, a single protein could serve as platform for the design of AbRxH possessing varying electrochemical and catalytic properties. Interestingly, nanofibrils of HET_{PFD} are highly stable in aqueous solution thanks to the numerous intra- and inter-molecular hydrogen bonds and salt-bridges between β-strands. The structure of the fibrils is known with atomistic resolution, [17] and it is not influenced by mutation of a few amino acids outside the hydrophobic core of the solenoid or the *C*-terminal semiflexible loop. [18] Also, their morphology can be controlled by tuning the electrostatic interaction of individual fibrils via pH and ionic strength of the solution. [19] [20]

We postulate that HET_{PFD} could serve as self-associating building block for the rational design of AbRxHs in which the position of artificial prosthetic group(s) along the fibril can be finely controlled by choosing the appropriate anchoring point in the polypeptide chain. In this manner, gel matrices could be engineered for mediated electron transfer (MET) from an electrode to an enzyme or for more complex electrocatalytic reactions involving multiple redox and catalytic sites.

Here we report a first example of such strategy, in which [NiFeSe]-hydrogenase from *Desulfomicrobium baculatum* (*Db*H-[NiFeSe]) [21] was wired to carbon electrodes via a self-assembled amyloid-based redox hydrogel prepared from a hybrid PFD. *Db*H-[NiFeSe] was selected because it has one of the highest activities toward the oxidation of H_2 among NiFe hydrogenases (TOF = 4000 s^{-1}), [21] and because, like other [NiFeSe]-hydrogenases, it is inactivated under oxidizing electrochemical conditions. The latter aspect will allow a comparison with previously reported Nernst buffers for this class of enzymes. [5, 22].

Results and Discussion

Synthesis and structure of redox nanofibrils

A mutant of HET_{PFD} possessing a single cysteine residue at the *N*-terminus and a His6 tag at the *C*-terminus ($CysHET_{PFD}$) was constructed as self-associating building block that can be selectively functionalized via sulfhydryl chemistry.[23] The protein does not contain Met residues and, at pH values near neutrality, Cys is alkylated by water-soluble benzyl bromide derivatives considerably faster than any other amino acid.[24]

Recombinant $CysHET_{PFD}$ (M_r = 9037.0 g mol^{-1}, theoretical pI = 7.24) was produced by heterologous overexpression in *E. Coli* and 80–140 mg of purified protein were obtained per litre of shake culture (i.e. 40–70 mg of per gram of wet cells; see SI).

Unfolded (monomeric) $CysHET_{PFD}$ was conjugated to bromobenzyl methyl viologen (40 eq.) by nucleophilic substitution under denaturing conditions (GuHCl 5M, pH 7.3, 20°C). Benzyl methyl viologen (BMV) was chosen as redox relay since viologen moieties undergo efficient electron transfer with hydrogenases either in freely diffusing [25] or polymer-bound forms. [26] Also, they display fast reaction kinetics with O_2, [27] thus enabling the design

of redox hydrogels that protect (bio)catalysts against oxygen damage (although protection from O_2 was not explored in this study). [22, 26d, 28]

After purification by affinity chromatography, MADI-TOF-MS analysis confirmed that the isolated protein (BMV-HET$_{PFD}$) featured a single benzyl methyl viologen, while its absorbance band at 260 nm is clearly visible in the UV-Vis spectrum (Figure S4). Self-association of the hybrid protein (0.13 mM in AcOH 1%) was induced by consecutive buffer exchange (citrate 20 mM pH 3.6, then HCl ~0.1 mM), and progress of fibrillation was monitored by circular dichroism though the appearance of a positive peak at 195 nm and a negative peak at 214 nm (Figure 1), both characteristic of the β-strand conformation predominant in amyloid structures.[29]

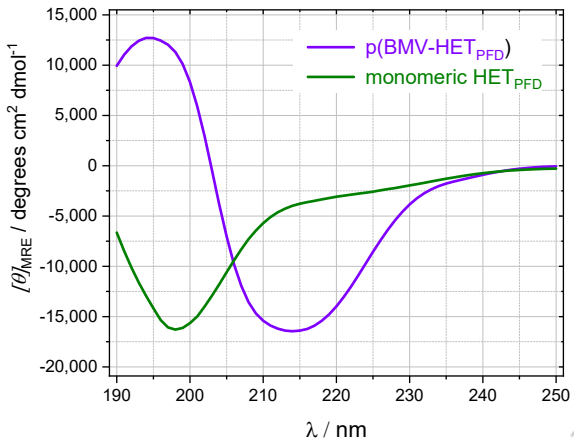

Figure 1. CD spectrum of p(BMV-HET$_{PFD}$) redox nanofibrils (0.1 mM HCl pH ~3.5) and of the unfolded prion-forming domain (AcOH 1% v/v pH 2.6) in the UV region. Upon polymerization, a transition occurs from a disordered conformation to one rich in β-strands, with a pronounced minimum at 214 nm. [29]

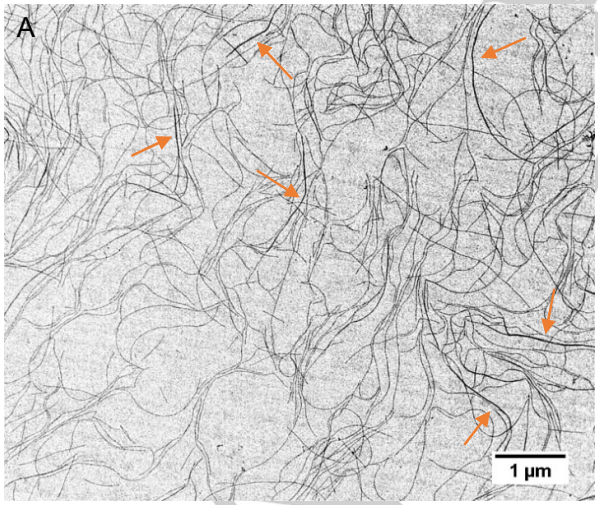

Figure 2. Low voltage TEM image of p(BMV-HET$_{PFD}$) in 0.1 mM HCl pH 3.5: the sample mostly consists of single-stranded fibrils with some double- and triple-stranded fibres, a few examples of which are indicated by arrows.

Fibrillation was complete after 23 hours and the length and morphology of the fibrils was observed by low voltage TEM without staining (Figure 4 a). Single-stranded fibrils of BMV-HET$_{PFD}$ - hereafter indicated as p(BMV-HET$_{PFD}$) - were predominant, but coexisted with double- and triple-stranded fibres resulting from lateral association. Measurement of a small sample of fibrils in TEM images (n=100) indicated that number average contour length was $L_n \cong 1.4$ µm (which corresponds to an average length / width aspect ratio of 350) and that fibrils were heterogeneous in length (0.2 µm ≤ L ≤ 3.7 µm, σ = 0.9 µm). The L_n value obtained by TEM is certainly underestimated, since long individual fibrils are more difficult to identify due to their tendency to intertwine and overlap with other fibrils; and because they often extend beyond the visualization area.

Starting from a 5-repeat structure of fibrils of HET-s(218-289) resolved by ssNMR (PDB 2RNM), [17b] a 12-repeat model for p(BMV-HET$_{PFD}$) fibrils was built by Molecular Dynamics simulation and energy minimization (see SI). As shown in Figure 3, benzyl-methyl-viologen groups are loosely aligned along the fibril axis and anchored at 9.4 Å intervals to the central β-solenoid via a flexible polypeptide chain 10 amino acids long. By exploring its conformational space in solution, the latter enables close encounters between redox relays of proteins that are up to four positions apart along the fibril axis, i.e. overcoming up to four consecutive functionalization defects in the fibril. This encounters support self-exchange reactions among the nanofibril-bound oxidized/reduced redox groups and, ultimately, MET between the hydrogenase and the electrode.

Figure 3. Structure of a p(BMV-HET$_{PFD}$) fibril. Different colours indicate different polypeptide chains; benzyl methyl viologen groups are shown in purple.

Amyloid-based redox hydrogels - AbRxHs

Nanofibrils of p(BMV-HET$_{PFD}$) expose a majority of acidic, basic, hydrophilic and positively charged residues on their surface (Figure S7), among which hydrophobic patches are interspersed. At pH < 4 and low ionic strength, lateral association is unfavourable due to electrostatic repulsion between positively charged fibrils and, at low concentration, a majority of single-stranded filaments are observed under these conditions (Figure 4a and Figure S6). At higher pH values though, net surface charge will be much diminished and electrostatic attraction between oppositely charged patches, as well as hydrophobic interaction between nonpolar patches, will lead to later association of nanofibrils into larger fibres and bundles. We hypothesised that, above a critical fibril overlap concentration, a sudden decrease in net surface charge would result in a 3D supramolecular network of entangled nanofibres of varying morphology, cross-linked by physical junction zones.

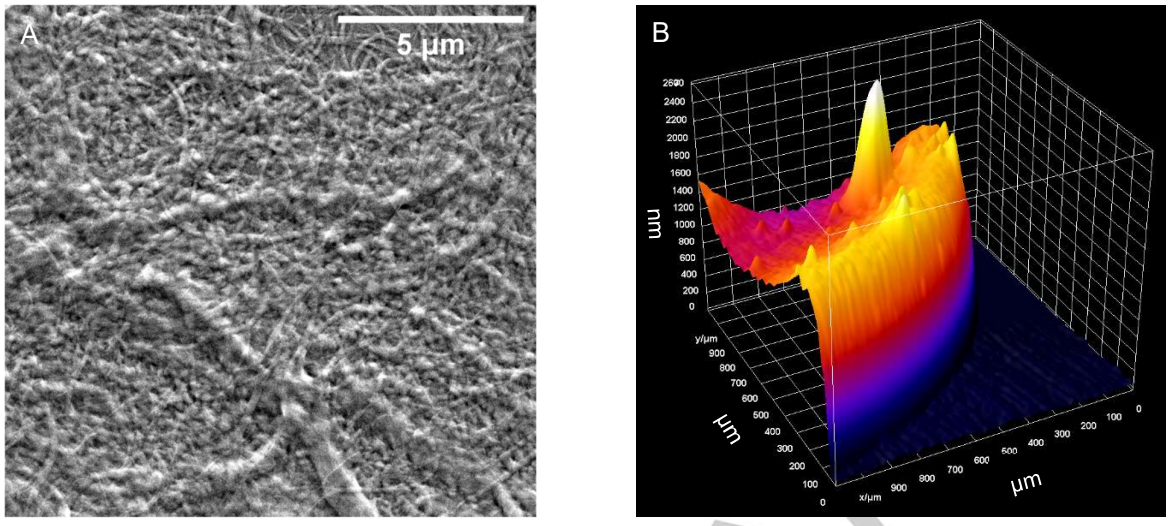

Figure 4. (a) SEM image of a dried single-layer p(BMV-HET$_{PFD}$) gel film formed on a glassy carbon electrode. b) Topography of an analogous film drop-cast on a borosilicate glass slide (drop volume 2.5 µL) as recorded by DHM. Films of circular shape ~2 mm in diameter were typically otained, and only quarter discs could be imaged by DHM. The scale of the z-axis is nm, whereas x and y axis are in µm.

The initial suspension of positively charged nanofibrils in 0.1 mM HCl was concentrated 5 ½ fold by ultrafiltration ($c_{final} \cong 3.8$ g L^{-1}), and films were prepared by drop casting 2.0 µL to 4.0 µL onto planar surfaces, followed by drying of the sessile droplet in the open atmosphere. Simple rehydration in the supporting electrolyte used for electrochemical experiments (TrisHCl 20-50 mM / NaCl 50 mM, pH 7.6) effected both later association of the fibrils into larger fibres and their physical cross-linking, yielding transparent hydrogel films. Figure 4a shows a SEM image of the dried gel coating a glassy carbon electrode: as expected, it is a dense and intricate network of fibres and bundles with lateral dimension of 100-150 µm and 400-700 µm, respectively.

The profile of the dried film before physical cross-linking was recorded by stylus profilometry and indicates a thickness varying from 1.7 µm to 3.0 µm with some accumulation of material both at the centre and at the outer rim of the circular deposit (drop volume 3.0 µL, film diameter 2.5 mm; Figure S15). Departure from a flat film morphology is often observed in films obtained by drop-casting methods and it is the result of a complex interplay between mass and heat transport processes taking place within the drying droplet. [30] In our case though, film inhomogeneity is much less pronounced than the "coffee-ring effect" reported for branched and dendritic viologen-polyethylenimine solutions drop-cast under similar non-gelling conditions. [31]

To gain a better insight into the morphology of swollen electroactive and electrocatalytic films, the topography of various AbRxHs was investigated by Digital Holographic Microscopy (DHM) in transmission mode. [32] DHM is a quantitative phase microscopy technique that enables full-field imaging of the structure and dynamics of transparent samples from a single recorded hologram. Vertical accuracy as low as a few tens of nanometers is achievable under adequate conditions. [32b].

Circular films 2 mm ±0.1 mm in diameter were obtained by drop-casting 2.0 µL of nanofibrils's suspension onto borosilicate glass slides (as measured by optical microscopy). Quarter films were imaged by DHM both in the dry and hydrogel state (Figure S17 and S18). Although surface energy and roughness of the glass slides used for DHM differ from that of GC, the radial profile obtained for a dry single-layer p(BMV-HET) film (Figure 4b) is similar to that observed by stylus profilometry with a peak-to-valley ratio of ~1.7. The fact that absolute thickness is smaller in the DHM experiment compared to stylus profilometry is probably the result of the smaller volume applied (2.0 µL vs 3.0 µL). Rehydration and cross-linking in the supporting electrolyte swelled the film without any variation in diameter, while the overall profile was maintained. This property is important for ensuring reproducibility of the coating process.

Electrochemistry and bioelectrocatalysis with AbRxHs

Cyclic voltammograms of p(BMV-HET$_{PFD}$) hydrogel films on Glassy Carbon (GC) and Edge Plane Pyrolytic Graphite (EPPG) electrodes (Figure 5 a,c) display a chemically reversible redox couple with half wave potential $E_{1/2}$ of -0.29 V and -0.28 V, respectively, at all tested scan rates; i.e. a value 0.12 V higher than the formal potential of the Vio^{++}/Vio$^{+\bullet}$ redox couple of free BMV in solution ($E_{1/2}$= -0.408 V). [33]

This shift to higher redox potentials was anticipated, having been consistently observed for redox polymers in which a viologen derivative is anchored to a positively charged macromolecular matrix. [26a, 26d, 31, 34] [35] It is due to the polyelectrolyte nature of the redox hydrogel, in which the electrostatic, excluded volume, and van der Waals interaction fields couple in a complex way and determine the free energy of the system.[36] As a result, the formal potential of viologen moieties in p(BMV-HET$_{PFD}$) hydrogels is 50 mV more positive than that of [4Fe-4S] clusters of *Db*H-[NiFeSe] (Figure S8), [21, 37] thus providing a sufficient driving force for ET between the hydrogenase and the redox matrix.

For modified GC electrodes, peak-to-peak separation (ΔE_p) at low scanning rates was ~50 mV, close to the 57 mV expected for a reversible monoelectronic diffusion-controlled redox system. [38]

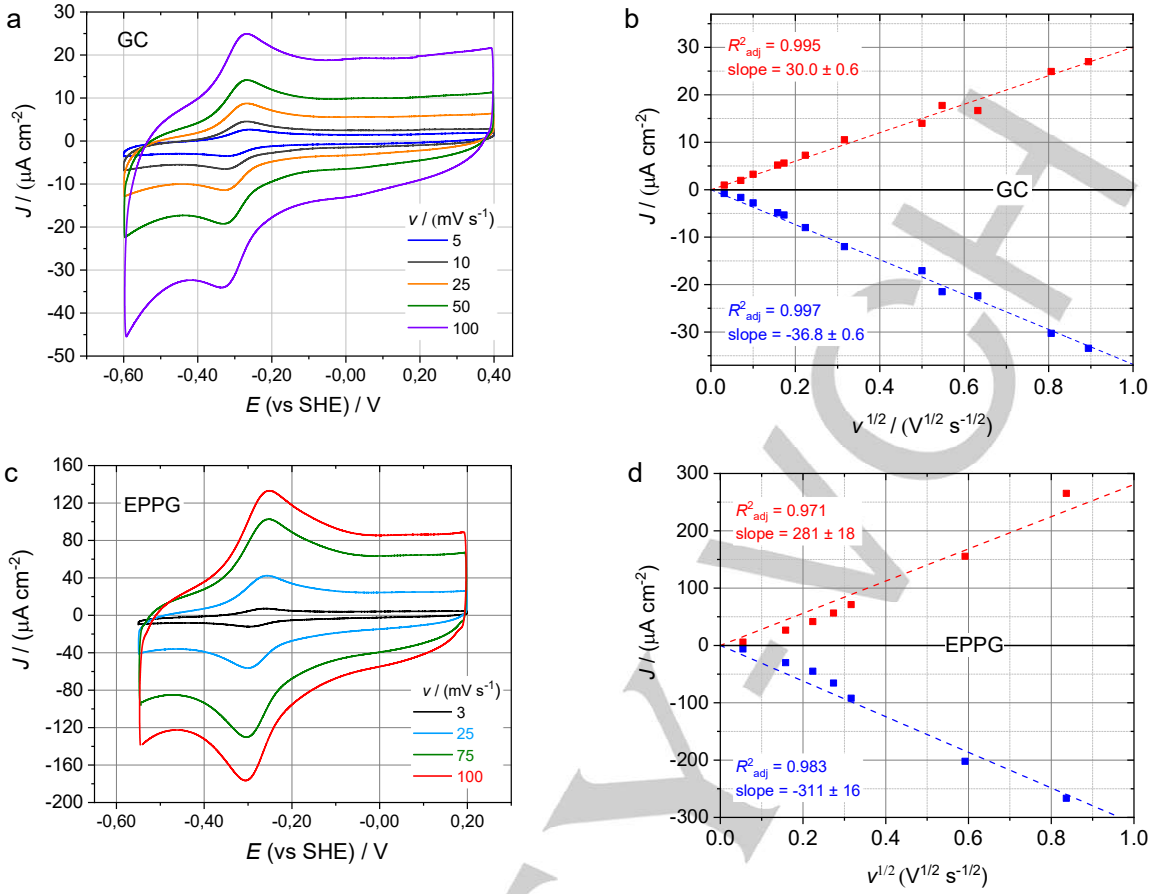

Figure 5. Cyclic voltammograms (a, c) and dependency of the cathodic and anodic currents on scan rate (b, d) for p(BMV-HET$_{PFD}$) hydrogel films on GC and EPPG electrodes. Background capacitive current was subtracted and the intercept of linear regression functions was forced through the origin. (See SI for more voltammograms). Conditions: 2 µL drop coating, supporting electrolyte TrisHCl 20 mM (GC) or 50 mM (EPPG) / NaCl 50 mM, pH 7.6.

At increasing scan rates, background-subtracted peak current densities J increased linearly with the square root of scan rate $v^{1/2}$ (Figure 5 b), indicating that electron transfer within the hydrogel film is governed by semi-infinite linear diffusion. [39] According to the Randles–Sevcik equation, the slope of the linear dependency scales as:

$$\text{slope} \propto C\left(\frac{D_{CT}}{T}\right)^{\frac{1}{2}} \qquad (1)$$

where C is concentration of redox species, D_{CT} is the apparent charge-transport diffusion coefficient, and T is temperature. The slope measured for the oxidation of Vio$^{+\bullet}$ moieties in p(BMV-HET$_{PFD}$) (3.0×10^{-5} A cm^{-2} V$^{-1/2}$s$^{1/2}$) is 5.1 times higher than what observed for rubredoxin in RdHET-based AbRxHs on GC.[13b] Since equilibrium concentration of protein units is expected to be similar in the two hydrogels, D_{CT} must be at least one order of magnitude higher in the biohybrid matrix. This result was expected in virtue of the smaller size - hence higher D_{phys} - of methylviologen as compared to rubredoxin.[40] Nonetheless, the implied D_{CT} is still 2 to 3 orders of magnitude lower than what reported for a methyl viologen-polyethylenimine hydrogel (D_{CT} = 4.7 x10^{-9} cm^2 s^{-1}).[28a] Possible explanations involve inter-wire charge transfer being hindered by limited surface contact and/or high distance; and the limited Brownian motion of large rigid nanofibers diminishing the collision frequency of redox sites. [40-41]

A different behaviour was observed for modified EPPG edge electrodes (Figure 5 c, d). Compared to analogous GC electrodes, higher current densities recorded at all scanning rates, but linear regression between peak current density J and $v^{½}$ is less convincing. The scaling of J with v is even poorer, thus excluding a surface-confined electron transfer process (Figure S10). Also, ΔE_p was 27 mV at a low scanning rate (v = 3 mV s^{-1}) and increased almost linearly with $v^{½}$ to reach 89 mV at 700 mV s^{-1} (Figure S9 d). Plainly, the electrochemistry of the film is more sophisticated than simple gradient-driven charge transport via electron self-exchange reactions between tethered redox centres. Probably the effect of counter-ion diffusion, ion pairing, water transport and nanofibers rearrangement becomes more pronounced at the current densities observed for EPPG electrodes.[42]

Bioelectrodes for H_2 oxidation were fabricated by imbedding [NiFeSe]-hydrogenase from *Desulfomicrobium baculatum* (*Db*H-[NiFeSe]) into the AbRxH films coating carbon electrodes. Two different protocols were implemented, which involved the same amount of enzyme being applied onto the electrode.

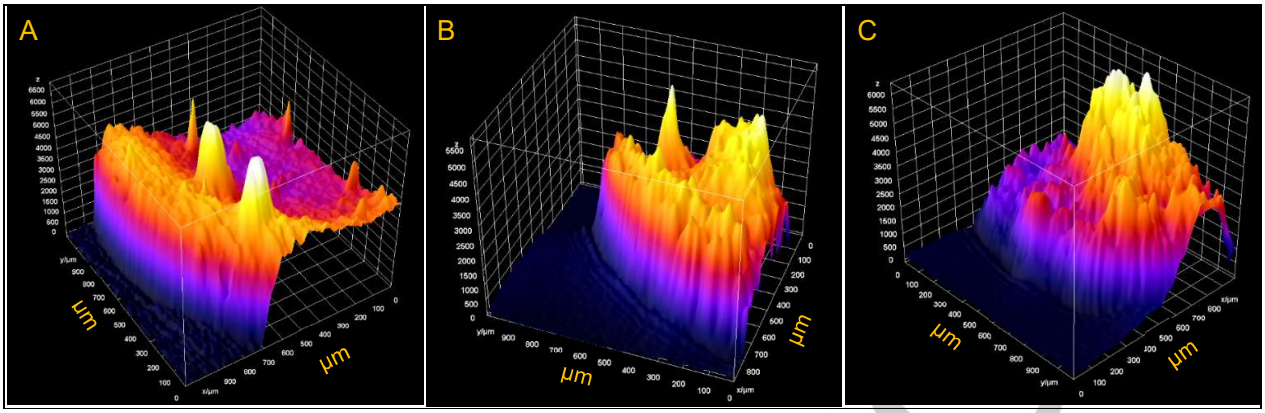

Figure 6. Topography of (A) single-layer electroactive p(BMV-HET$_{PFD}$), and (B) single-layer and (C) double layer p(BMV-HET$_{PFD}$) / *Db*H-[NiFeSe] bioelectrocatalytic hydrogel films drop-cast on a glass slide. The vertical the scale is the same for all graphs, but it is in arbitrary units, whereas x and y axis are in µm.

In the first protocol, single-layer bioelectrocatalytic films were obtained by drop casting 3 µL of p(BMV-HET$_{PFD}$) fibrils suspension on the electrode followed by drying in the open atmosphere. The dry film was then swollen with 2 µL of buffered *Db*H-[NiFeSe] solution (pH 7.6), which also effected physical cross-linking by changing the surface charge of the nanofibrils. We postulated that, during the swelling process, part of the negatively charged enzyme (pI = 5.7) would penetrate the nanofibers mesh and be entrapped by electrostatic interaction with the multiple positive charges on the nanofibers.[43] Close inspection of the swelling process, however, revealed that most of the enzyme solution was not absorbed by the film at equilibrium, and was effectively wasted.

In an attempt to increase the efficiency of immobilization, a second protocol was tested in which the enzyme was pre-mixed with an equal volume of nanofibril suspension before being applied to electrode. Hence, double-layer electrocatalytic films were prepared by drop coating a first layer of p(BMV-HET$_{PFD}$) as describe above, followed by drop casting 2µL or 4 µL of a 1:1 mixture of p(BMV-HET$_{PFD}$) / *Db*H-[NiFeSe] on the top of it, drying in the open atmosphere and immersion in the working electrolyte to complete electrostatic cross-linking.

Topography of the electroactive and bioelectrocatalytic hydrogel films obtained in this manner is shown in Figure 6. Compared to a single-layer p(BMV-HET$_{PFD}$) film (a), the addition of enzyme resulted in an accumulation of material at the centre of the film disk (b and c), as indicated by the increased thickness, while the footprint of the film remained unchanged. The effect was particularly pronounced for double-layer electrocatalytic films due to the further addition of p(BMV-HET$_{PFD}$) fibres.

Figure 7 depicts cyclic voltammograms obtained under Ar (solid line) and H_2 atmosphere (dashed line) for GC (a) and EPPG electrodes (b) modified with p(BMV-HET$_{PFD}$) / *Db*H-[NiFeSe] hydrogel coatings. Experiments were realized under quiescence conditions with a supporting electrolyte solution saturated either with Ar or with H_2; while gentle flushing of the cell head-space with the appropriate gas was maintained throughout the experiment.

Under Ar atmosphere, the redox couple for the first viologen reduction was clearly observed with double-layer electrodes (Figure 7a,b and Figure S12), but the anodic wave was more intense than the cathodic one, possibly due to rapid oxidation of H_2 slowly generated in-situ at low potentials. In the case of single-layer GC electrodes, a small anodic catalytic wave was indeed visible (H^+ reduction).

Under H_2 atmosphere, pronounced catalytic waves were observed that are centred at the formal potential of the viologen electron relays. Since the latter is 150 to 170 mV more positive than the $2H^+$ / H_2 couple ($E^{\circ`}_{H+/H2}$ = -0.449 V at pH 7.6), the MET chain involving BMV moieties is limiting the turnover of the enzyme and DET can be excluded. According to the model of Léger, [44] the active site of a multicenter redox enzyme feels the potential of a ET relay under the condition that the ET chain limits the enzymatic turnover. In this case, the ET relay acts as a Nernst buffer and protects the enzyme from high potential deactivation. However, if enzymatic turnover is limiting, fast ET chains involving artificial electron relays will display the same properties as the direct ET of enzymes directly adsorbed to electrodes, i.e. a catalytic wave centred on the redox potential of the enzyme's active site or of the substrate. In this case, protection from high potential would not be achieved.

With p(BMV-HET$_{PFD}$)-modified electrodes, no oxidative inactivation of the enzyme took place at applied potentials as high as +0.40 V. By contrast, when a similar experiment was conducted with the enzyme co-immobilized with an electroinactive amyloid-based hydrogel of p(HET$_{PFD}$), a small anodic wave started at -0.42 V, but leveled off at -0.20 V due to oxidative inactivation (Figure S8).[5] Hence, the AbRxH acts as a Nernst buffer and protects the hydrogenase from high potential deactivation.

Single- and double-layer coatings of GC electrodes lead to similar catalytic current profiles (Figure 7 a, series at 25°C), with a monotonic increase of current density with applied potential that slows down above -0.15 V but never reaches a steady-state. This behaviour is independent of operating temperature and suggests that H_2 diffusion is not limiting catalytic current. In terms of electrocatalytic efficiency, then, the two coating protocols seem to be equivalent.

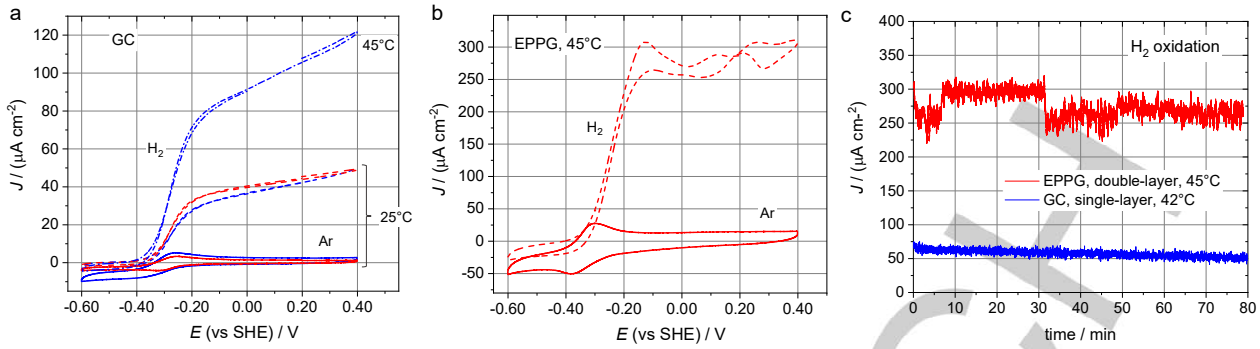

Figure 7. Cyclic voltammograms under quiescent conditions of modified GC (a) and EPPG (b) electrodes (scan rate 10 mV s^{-1}). Curves for single-layer (blue series) and double–layer (red series) p(BMV-HET$_{PFD}$) / *Db*H-[NiFeSe] hydrogel coatings under Ar (solid line) or H_2 atmosphere (dashed line) are shown. (c) Chronoamperometry at *E* = +0.20 V (GC) and +0.00 V (EPPG) under H_2 atmosphere. Coating volumes: GC single-layer, 3µL fibrils + 2µL enzyme; GC double-layer, 4µL fibrils + 4µL mix; EPPG double-layer, 3µL fibrils + 2µL mix. Supporting electrolyte TrisHCl 20 mM (50 mM for chronoamperometry GC) / NaCl 50 mM, pH 7.6.

It is worth noting that current density due to H_2 oxidation at +0.40 V and 45 °C was 6 times higher than previously obtained at 60°C with [NiFe] hydrogenase from *Aquifex aeolicus* embedded in RdHET-based AbRxH (a GC electrode was used in both cases),[13a] thus confirming the relevance of the new bioelectrode design. Under continuous turnover conditions at +0.20 V, a slow but steady decline in catalytic current was observed, and after 80 min. only ~65 % of the initial activity remained (Figure 7c). A complementary experiment (Figure S13) showed that the loss in catalytic current matched the reduction in charge exchanged during cyclic voltammetry for the reduction/oxidation of viologen moieties in the matrix. Excluding hydrolysis or degradation of BMV groups, it follows that gradual exfoliation and/or disassembly of the hydrogel is the main cause for the limited stability of the electrode over time. Enzyme inactivation and/or diffusion away from the electrode surface cannot be exclude though.

Results with modified EPPG electrodes were rather different (Figure 7 b). For applied potentials higher than -0.15 V, the monotonic increase of current density stopped, and *J* started oscillating around a plateau of ~270 µA cm^{-2}. This value is over three-times higher than the current density recorded for modified GC electrodes at the same potential (*E* = -0.15 V) and temperature (45 °C), the only other difference being the coating protocol – which was previously found to have little influence on catalytic currents (see Figure 7 a, series at 25°C).

Current density fluctuations of ± 7% with a period of ~1 min were also recorded in chronoamperometric experiments under continuous H_2 oxydation conditions, but average current did not decline over an 80 min period, thus proving the robustness of the bioelectrode on this time scale (Figure 7c). The fluctuations in *J* at high potential might be due to local fluctuations in substrate transport, pH and/or nanowires morphology that do not take place at the slower reaction rates achieved with GC electrodes.

Conclusion

An artificial amyloid-based redox hydrogel was designed for mediating electron transfer from a [NiFeSe] hydrogenase to an electrode. Starting from a mutated prion-forming domain of fungal protein HET-s, a hybrid redox protein was synthesized that is capable of self-assembling into structurally homogenous nanofibrils in a predictable way. Molecular modelling confirmed that redox groups are loosely aligned along the fibril's axis and tethered to the central solenoid via a long flexible polypeptide chain. By exploring its conformational space in solution, the latter enables self-exchange reactions among the fibril-bound oxidized/reduced redox groups and, ultimately, mediates electron transport between the hydrogenase and the electrode.

At high concentration, a sudden change in surface charge of the fibrils leads to their lateral association into protein nanowires and physical cross-linking through non-covalent interactions. This property was exploited to prepare redox hydrogel films that are capable of immobilizing an hydrogenase at the surface of carbon electrodes under mild conditions. Topography investigations revealed some accumulation of material both at the centre and at the outer rim of the circular deposit, but no "coffee-ring effect".

Based on these properties, new bioelectrodes for the electrocatalytic oxidation of H_2 were fabricated that afforded catalytic current densities of up to 270 µA cm^{-2} under quiescent conditions for over one hour. Gradual desorption and/or disassembly of the hydrogel appears to be the main factor limiting electrode stability over time, and further work is needed in this direction.

Although conductive nanofibers featuring aryl-viologen groups were recently obtained by the self-assembly of a short peptide,[45] their ability to mediate electron transfer to an enzyme was not investigated. What is more, nanofibrils based on HET$_{PFD}$ offer a wide scope for the rational design of monodimensional nanomaterials though site-directed mutagenesis and post-expression functionalization of the monomeric prion-forming domain, thanks to their intrinsic robustness, structural complexity and homogeneity.

Acknowledgements

This work has been partially supported by Labex ARCANE and CBH-EUR-GS (ANR-17-EURE-0003). We thank the NanoBio-ICMG Platform (FR 2607, Grenoble) for granting access to the Electron Microscopy and Mass Spectrometry facilities. This work used the platforms of the Grenoble Instruct-ERIC centre (ISBG; UMS 3518 CNRS-CEA-UGA-EMBL), part of the Grenoble Partnership for Structural Biology (PSB), supported by FRISBI

(ANR-10-INBS-05-02) and GRAL, financed by the University Grenoble Alpes graduate school (*Ecoles Universitaires de Recherche*) CBH-EUR-GS (ANR-17-EURE-0003). Finally, we thank Dr. S. Ménage for useful discussions and suggestions.

Keywords: hybrid prion forming domain • supramolecular polymer • protein nanowire • redox hydrogel• bioelectrocatalysis

[1] a) J. Masa, W. Schuhmann, *Nano Energy* **2016**, *29*, 466-475; b) H. Chen, F. Dong, S. D. Minteer, *Nature Catalysis* **2020**.

[2] D. P. Hickey, R. D. Milton, M. Rasmussen, S. Abdellaoui, K. Nguyen, S. D. Minteer, in *Electrochemistry: Volume 13, Vol. 13*, The Royal Society of Chemistry, **2016**, pp. 97-132.

[3] a) F. A. Armstrong, H. A. O. Hill, N. J. Walton, *Accounts of Chemical Research* **1988**, *21*, 407-413; b) A. A. Karyakin, *Bioelectrochemistry* **2012**, *88*, 70-75.

[4] K. A. Vincent, A. Parkin, F. A. Armstrong, *Chemical Reviews* **2007**, *107*, 4366-4413.

[5] S. Gentil, S. M. Che Mansor, H. Jamet, S. Cosnier, C. Cavazza, A. Le Goff, *ACS Catalysis* **2018**, *8*, 3957-3964.

[6] A. Heller, *Current Opinion in Chemical Biology* **2006**, *10*, 664-672.

[7] A. Ruff, *Current Opinion in Electrochemistry* **2017**, *5*, 66-73.

[8] a) A. Kumari, B. Ahmad, *RSC Advances* **2019**, *9*, 37424-37435; b) B. H. Pogostin, S. Linse, U. Olsson, *Langmuir* **2019**, *35*, 16536-16544.

[9] a) M. Wehner, F. Würthner, *Nature Reviews Chemistry* **2020**, *4*, 38-53; b) S. Koutsopoulos, *Journal of Biomedical Materials Research Part A* **2016**, *104*, 1002-1016; c) G. Fichman, E. Gazit, *Acta Biomaterialia* **2014**, *10*, 1671-1682; d) J. D. Tang, C. Mura, K. J. Lampe, *J. Am. Chem. Soc.* **2019**, *141*, 4886-4899; e) L. Yang, H. Li, L. Yao, Y. Yu, G. Ma, *ACS Omega* **2019**, *4*, 8071-8080; f) S. Das, R. Kumar, N. N. Jha, S. K. Maji, *Advanced Healthcare Materials* **2017**, *6*, 1700368.

[10] R. Wang, X. Yang, L. Cui, H. Yin, S. Xu, *Biomolecules* **2019**, *9*.

[11] A. J. Baldwin, R. Bader, J. Christodoulou, C. E. MacPhee, C. M. Dobson, P. D. Barker, *J. Am. Chem. Soc.* **2006**, *128*, 2162-2163.

[12] D. Leys, N. S. Scrutton, *Current Opinion in Structural Biology* **2004**, *14*, 642-647.

[13] a) S. Rengaraj, R. Haddad, E. Lojou, N. Duraffourg, M. Holzinger, A. Le Goff, V. Forge, *Angew. Chem., Int. Ed.* **2017**, *56*, 7774-7778; b) L. Altamura, C. Horvath, S. Rengaraj, A. Rongier, K. Elouarzaki, C. Gondran, A. L. B. Maçon, C. Vendrely, V. Bouchiat, M. Fontecave, D. Mariolle, P. Rannou, A. Le Goff, N. Duraffourg, M. Holzinger, V. Forge, *Nature Chemistry* **2017**, *9*, 157-163.

[14] A. Balguerie, S. D. Reis, C. Ritter, S. Chaignepain, B. Coulary‐Salin, V. Forge, K. Bathany, I. Lascu, J. M. Schmitter, R. Riek, S. J. Saupe, *The EMBO Journal* **2003**, *22*, 2071-2081.

[15] A. Balguerie, S. Dos Reis, B. Coulary-Salin, S. Chaignepain, M. Sabourin, J. M. Schmitter, S. J. Saupe, *Journal of Cell Science* **2004**, *117*, 2599-2610.

[16] P. Hosseinzadeh, Y. Lu, *Biochim Biophys Acta* **2016**, *1857*, 557-581.

[17] a) C. Ritter, M.-L. Maddelein, A. B. Siemer, T. Luhrs, M. Ernst, B. H. Meier, S. J. Saupe, R. Riek, *Nature* **2005**, *435*, 844-848; b) C. Wasmer, A. Lange, H. Van Melckebeke, A. B. Siemer, R. Riek, B. H. Meier, *Science* **2008**, *319*, 1523-1526.

[18] a) A. Daskalov, M. Gantner, M. A. Walti, T. Schmidlin, C. N. Chi, C. Wasmer, A. Schutz, J. Ceschin, C. Clave, S. Cescau, B. Meier, R. Riek, S. J. Saupe, *Plos Pathogens* **2014**, *10*; b) W. Wan, G. Stubbs, *PNAS* **2014**, *111*, 5201-5206.

[19] R. Sabaté, U. Baxa, L. Benkemoun, N. Sánchez de Groot, B. Coulary-Salin, M.-I. Maddelein, L. Malato, S. Ventura, A. C. Steven, S. J. Saupe, *Journal of Molecular Biology* **2007**, *370*, 768-783.

[20] W. Close, M. Neumann, A. Schmidt, M. Hora, K. Annamalai, M. Schmidt, B. Reif, V. Schmidt, N. Grigorieff, M. Fändrich, *Nature Communications* **2018**, *9*, 699.

[21] A. Parkin, G. Goldet, C. Cavazza, J. C. Fontecilla-Camps, F. A. Armstrong, *Journal of the American Chemical Society* **2008**, *130*, 13410-13416.

[22] A. Ruff, J. Szczesny, S. Zacarias, I. A. C. Pereira, N. Plumeré, W. Schuhmann, *ACS Energy Letters* **2017**, *2*, 964-968.

[23] a) G. A. Grant, in *Current Protocols in Protein Science*, John Wiley & Sons, Inc., **2001**; b) C. D. Spicer, B. G. Davis, *Nature Communications* **2014**, *5*, 4740; c) O. Boutureira, G. J. L. Bernardes, *Chemical Reviews* **2015**, *115*, 2174-2195.

[24] a) G. A. Rogers, N. Shaltiel, P. D. Boyer, *J. Biol. Chem.* **1976**, *251*, 5711-5717; b) E. Calce, M. Leone, L. Monfregola, S. D. Luca, *Organic Letters* **2013**, *15*, 5354-5357.

[25] H. Tatsumi, K. Takagi, M. Fujita, K. Kano, T. Ikeda, *Analytical Chemistry* **1999**, *71*, 1753-1759.

[26] a) L. H. Eng, M. Elmgren, P. Komlos, M. Nordling, S.-E. Lindquist, H. Y. Neujahr, *The Journal of Physical Chemistry* **1994**, *98*, 7068-7072; b) A. L. De Lacey, M. Detcheverry, J. Moiroux, C. Bourdillon, *Biotechnology and Bioengineering* **2000**, *68*, 1-10; c) A. A. Karyakin, D. V. Vinogradova, S. V. Morozov, E. E. Karyakina, *Electrochimica Acta* **2010**, *55*, 7696-7700; d) N. Plumeré, O. Rüdiger, A. A. Oughli, R. Williams, J. Vivekananthan, S. Pöller, W. Schuhmann, W. Lubitz, *Nature Chemistry* **2014**, *6*, 822.

[27] a) J. A. Farrington, M. Ebert, E. J. Land, K. Fletcher, *Biochimica Et Biophysica Acta* **1973**, *314*, 372-381; b) R. N. Thorneley, *Biochimica Et Biophysica Acta* **1974**, *333*, 487-496; c) Q. Lin, Q. Li, C. Batchelor-McAuley, R. G. Compton, *Physical Chemistry Chemical Physics* **2013**, *15*, 7760-7767.

[28] a) V. Fourmond, S. Stapf, H. Li, D. Buesen, J. Birrell, O. Rüdiger, W. Lubitz, W. Schuhmann, N. Plumeré, C. Léger, *Journal of the American Chemical Society* **2015**, *137*, 5494-5505; b) A. A. Oughli, F. Conzuelo, M. Winkler, T. Happe, W. Lubitz, W. Schuhmann, O. Rüdiger, N. Plumeré, *Angewandte Chemie International Edition* **2015**, *54*, 12329-12333; c) A. A. Oughli, A. Ruff, N. P. Boralugodage, P. Rodríguez-Maciá, N. Plumeré, W. Lubitz, W. J. Shaw, W. Schuhmann, O. Rüdiger, *Nature Communications* **2018**, *9*, 864; d) J. Szczesny, N. Marković, F. Conzuelo, S. Zacarias, I. A. C. Pereira, W. Lubitz, N. Plumeré, W. Schuhmann, A. Ruff, *Nature Communications* **2018**, *9*, 4715; e) H. Li, D. Buesen, S. Dementin, C. Léger, V. Fourmond, N. Plumeré, *Journal of the American Chemical Society* **2019**, *141*, 16734-16742.

[29] S. M. Kelly, T. J. Jess, N. C. Price, *Biochimica et Biophysica Acta (BBA) - Proteins and Proteomics* **2005**, *1751*, 119-139.

[30] a) D. Willmer, K. A. Baldwin, C. Kwartnik, D. J. Fairhurst, *Physical Chemistry Chemical Physics* **2010**, *12*, 3998-4004; b) H. Hu, R. G. Larson, *The Journal of Physical Chemistry B* **2006**, *110*, 7090-7094; c) M. Anyfantakis, D. Baigl, *ChemPhysChem* **2015**, *16*, 2726-2734; d) R. D. Deegan, O. Bakajin, T. F. Dupont, G. Huber, S. R. Nagel, T. A. Witten, *Nature* **1997**, *389*, 827-829; e) R. D. Deegan, O. Bakajin, T. F. Dupont, G. Huber, S. R. Nagel, T. A. Witten, *Physical Review E* **2000**, *62*, 756-765.

[31] H. Li, D. Buesen, R. Williams, J. Henig, S. Stapf, K. Mukherjee, E. Freier, W. Lubitz, M. Winkler, T. Happe, N. Plumeré, *Chemical Science* **2018**, *9*, 7596-7605.

[32] a) P. Marquet, B. Rappaz, P. J. Magistretti, E. Cuche, Y. Emery, T. Colomb, C. Depeursinge, *Opt. Lett.* **2005**, *30*, 468-470; b) B. Rappaz, P. Marquet, E. Cuche, Y. Emery, C. Depeursinge, P. J. Magistretti, *Opt. Express* **2005**, *13*, 9361-9373.

[33] C. L. Bird, A. T. Kuhn, *Chemical Society Reviews* **1981**, *10*, 49-82.

[34] a) T. Nakahira, M. Graetzel, *J. Phys. Chem.* **1984**, *88*, 4006-4010; b) T. Janoschka, N. Martin, U. Martin, C. Friebe, S. Morgenstern, H. Hiller, M. D. Hager, U. S. Schubert, *Nature* **2015**, *527*, 78-81.

[35] To the best of our knowledge, the sole exception is a paper by Willner et all., in which a 0.25V shift toward more negative potentials is reported for a viologen-polyethylenimine system at pH 7. The shift decreases monotonically with decreasing pH and vanishes at pH = 1. The authors speculate that in neutral and basic solutions, electron-donating amino groups of the polymer backbone can form donor-acceptor charge-transfer complexes with the bipyridinium units, thereby transforming the redox groups into relatively electron-rich entities that require more negative potentials for their reduction. By contrast, in their recent and extensive work on branched and dendritic viologen-polyethylenimine hydrogels, a ~0.15 V shift toward more potentials was systematically observed by Lubitz, Schuhmann and Plumeré.

[36] M. Tagliazucchi, E. J. Calvo, in *Chemically Modified Electrodes* (Eds.: R. C. Alkire, D. M. Kolb, J. Lipkowski, P. N. Ross), John Wiley & Sons, Inc., **2009**, pp. 57-115.

[37] M. Teixeira, I. Moura, G. Fauque, D. V. Dervartanian, J. Legall, H. D. Peck Jr, J. J. G. Moura, B. H. Huynh, *European Journal of Biochemistry* **1990**, *189*, 381-386.

[38] J. M. Savéant, C. Costentin, *Elements of Molecular and Biomolecular Electrochemistry: An Electrochemical Approach to Electron Transfer Chemistry*, John Wiley and Sons, Hoboken, NJ, USA, **2019**.

[39] A. J. Bard, L. R. Faulkner, *Electrochemical Methods: Fundamentals and Applications, 2nd Edition*, John Wiley & Sons, **2001**.

[40] K. Sato, R. Ichinoi, R. Mizukami, T. Serikawa, Y. Sasaki, J. Lutkenhaus, H. Nishide, K. Oyaizu, *Journal of the American Chemical Society* **2018**, *140*, 1049-1056.

[41] L. Bello, C. E. Sing, *Macromolecules* **2020**, *53*, 7658-7671.

[42] a) Lyons, *Transport and Kinetics in Electroactive Polymers*, **1996**; b) G. Inzelt, in *Encyclopedia of Electrochemistry*, Wiley‐VCH, **2007**, pp. 651-683.

[43] Note that the BMV moiety contributes two permanent positive charges to each BMV-HET protein.

[44] C. Léger, F. Lederer, B. Guigliarelli, P. Bertrand, *Journal of the American Chemical Society* **2006**, *128*, 180-187.

[45] D. E. Clarke, M. Olesińska, T. Mönch, B. Schoenaers, A. Stesmans, O. A. Scherman, *Chemical Communications* **2019**, *55*, 7354-7357.

Entry for the Table of Contents

Insert graphic for Table of Contents here. ((Please ensure your graphic is in **one** of following formats))

((max. width: 5.5 cm; max. height: 5.0 cm))

Please delete this box prior to submission

((max. width: 11.5 cm; max. height: 2.5 cm))

Please delete this box prior to submission

Insert text for Table of Contents here. ((The Table of Contents text should give readers a short preview of the main theme of the research and results included in the paper to attract their attention into reading the paper in full. The Table of Contents text **should be different from the abstract** and should be no more than 450 characters including spaces.))